Organic Carbon transport model of abandoned river channels - A motif for floodplain geomorphology influencing biogeochemical swaying of arsenic

Devanita Ghosh [a,*], Santosh Kumar [b], Marinus Eric Donselaar [b,c], Cynthia Corroto [d], Ashok K. Ghosh [e]

[a] Laboratory of Biogeochem-mystery, Centre for Earth Sciences, Indian Institute of Science, Bengaluru 560012, India
[b] Department of Geoscience and Engineering, Delft Univ. of Technology, P.O. Box 5048, 2600 GA Delft, the Netherlands
[c] Department of Earth and Environmental Sciences, Division of Geology, KU Leuven, Celestijnenlaan 200E, B-3001 Leuven, Belgium
[d] Centro de Estudios Transdisciplinarios del Agua (CETA), Facultad de Ciencias Veterinarias, Universidad de Buenos Aires, Argentina
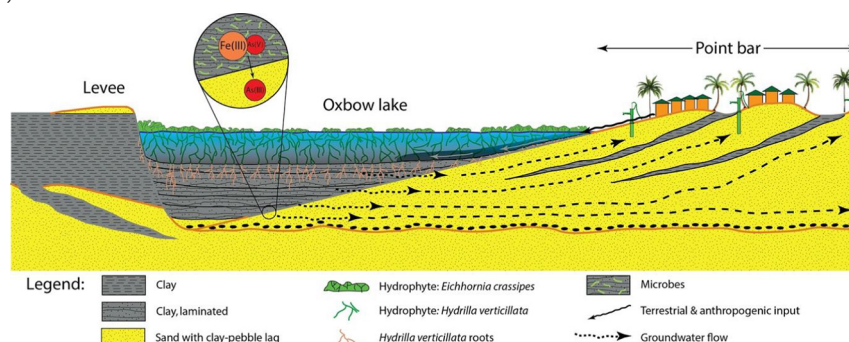[e] Mahavir Cancer Sansthan and Research Centre, 4th Floor Phulwari Sharif, Patna 801505, India

HIGHLIGHTS

- Top-down multidisciplinary analyses to study abandoned river channels
- Remote sensing based analysis revealing vegetation annual dynamics
- Organic carbon compound classes: distribution and preservation
- Microbiological metabolism of OC from different sources
- Microbial reductive dissolution of Fe (*oxy*)hydroxides associated As

GRAPHICAL ABSTRACT

Summarizes the manuscript, where characterization [Metadata: Remote sensing, Chemical and Biological] and possible role of OC from terrestrial, anthropogenic and hydrophytes [in Green] has been studied in details. Further investigation suggests these OC-burials in lake clay beds [in Grey], sustains the microbes [in light Green], which are responsible for reduction of Fe(III) [in Orange] and As(V) [in Red] and mobilization of As(III), which is transported to the villages located on point bars during groundwater abstraction (dotted lines).

ARTICLE INFO

ABSTRACT

Meandering-river geomorphology, forming abandoned channels/lakes with organic carbon-burial and microbial reductive dissolution, play many crucial roles in controlling arsenic (As) fluxes in sinks such as contaminated aquifers of riverine alluvial plains across the world. Suhiya oxbow-lake in the middle alluvial plain of the River Ganga, was selected as the natural laboratory. A top-down multidisciplinary approach was chosen employing satellite imagery to analyse the annual oxbow-lake surface vegetation dynamics (*Eichhornia* and *Hydrilla*). Side-scan sonar profiles across two oxbow lakes along with River Ganga core data and vintage topographical maps, estimated the lake-sedimentation rate of 9.6 cm/yr. Organic carbon [amino acids, aromatics, lingo-phenols and lipids hydrocarbons] infiltration-based on hydrophobicity and molecular-mass was detected at different depths along the water and sedimentary column. Elemental analysis showed lake surface to groundwater the As conc. varied from (0.37 to 185 μg/l). A microbial diversity based study showed that large sized photoautotrophs *Nostoc*, *Anabaena* are replaced by Fe-oxido-

* Corresponding author.
E-mail address: devanita@iisc.ac.in (D. Ghosh).

Biomarkers
Remote sensing

reducing As-metabolizing bacteria e.g. *Acidovorax*, *Dechloromonas* and enteric organisms e.g. *Enterobacter*, *Salmonella* at bottom of water column. Based on these inferences, a conceptual organic carbon transport model was constructed to understand the preferential preservation and microbial diagenesis resulting in mobilization of As and other geogenic elements.

1. Introduction

Toxic levels of arsenic (As; >10 μg/l; WHO, 2011) in drinking and irrigation water sources affect the health of millions of people across the globe (Guha Mazumder, 2003; Chikkanna et al., 2019; Kavil et al., 2020). Holocene alluvial plains worldwide can accumulate high concentrations of As in shallow Holocene aquifers (Mukherjee et al., 2009; Sahu and Saha, 2015). Arsenic is sourced in orogenic mountain belts upstream from the alluvial plains and, upon weathering of the orogenic rocks, is primarily transported in solid-state form in sediment to the depositional sinks. Göd and Zemann (1999) documented brecciated marbles in the Austrian Alps as primary As source; Horton et al. (2001) and Campbell et al. (2004) described hydrothermal As enrichment of calcite veins in altered fault rocks in Alpine Faults in New Zealand; multiple examples of As-enriched magmatic rocks are given by Mukherjee et al. (2014), and Tapia et al. (2019) described volcanic rocks, salts and thermal waters from the Altiplano Basin in South America as As-containing source rock. By contrast, concentrations of dissolved As in surface water are very low or even below the detection limit, in comparison with aquifer concentrations (Baig et al., 2000; BSRDC Ltd., 2016). The difference suggests that As is released *in situ* from its solid state in the alluvial-plain sediment, and subsequently migrates into the aquifer (Sahu and Saha, 2015; Donselaar et al., 2017; Ghosh and Bhadury, 2018). Notorious examples of highly As-polluted aquifers are in the alluvial plains of meandering rivers such as the Mekong River, Cambodia and Red River, Vietnam (Berg et al., 2007), Pearl River, China (Huang et al., 2011), Río Dulce River, Argentina (Bhattacharya et al., 2006; Bundschuh et al., 2004), Pazña River, Bolivia (Ramos et al., 2014), Meghna River, Bangladesh (Bhattacharya et al., 2002) and Ganga and Brahmaputra Rivers, India (Bhattacharya et al., 1997). The meandering-river geomorphology is the common denominator of all As-contaminated flood basins (Donselaar et al., 2017).

The hypothesis stating that the cause of high As levels is due to extensive pumping and drawdown of the groundwater table leading to oxidation and As release, has been highly controversial. However, seasonal alteration in the rates of pumping has been shown to contaminate topsoil and critical food crops (Kavil et al., 2020). A link between groundwater extraction from meandering-river point bars and As mobilization at the clay-sand interface between point bar and attached abandoned, sediment-filled meander loop (or: *clay plug*) has been suggested earlier (Fig. 1) (Sahu and Saha, 2015; Donselaar et al., 2017).

The clay-plug sediment is a cocktail of organic matter input from the terrestrial sources, oxbow-lake flora and fauna, and suspension-load of clay and silt sediment introduced by the main river channel during monsoon flooding periods. The surface-derived modern organic carbon (OC) input (usually <60 yr), is suggested to be the key player in the elemental fluxes of shallow aquifers systems (Lawson et al., 2013). The OC from terrestrial sources can act as electron donor for microbial metabolism and reductive dissolution of As-bearing Fe(II) oxy-hydroxides (Ghosh and Bhadury, 2018). A large number of efforts are been undertaken to identify the sources of OC which drives the As release that remains debatable. The contribution of peat deposits as sedimentary organic carbon (SOC) in such depositional environments has been studied as one of the potential source of bioavailable SOC in aquifers (Rowland et al., 2006; Ghosh et al., 2015a, 2018).

Oxbow lakes are monomictic (complete mixing occurs usually during floods) standing bodies of water, with thermal and redox stratification where perennial aquatic macrophytes such as *Azolla filiculoides* (free floating), *Eichhornia crassipes* (floating) and *Hydrilla verticillata* (submerged) along with animal life (zooplanktons) thrive and contribute to the high organic matter ratio in the lake sediment (Lawson et al., 2013; Ghosh and Biswas, 2015; Ghosh et al., 2017). The infiltration and deposition of the organic molecules through the water column depends on the physico-chemistry, reactivity and diagenetic alteration by biological processes and is conceptualized into a chromatography model in this paper.

The objectives of this paper are to i) identify the key organic carbon input in the oxbow lake, ii) understand the annual dynamics of the organic carbon sources (such as macrophytes), iii) understand the role of microbial metabolism of different C-compound classes in controlling As mobilization, and iv) build a conceptual model of organic molecular distribution and the controlling processes. To achieve the objectives, the Ganga River floodplain in Bhojpur District, Bihar, India (25° 6631″ N, 84° 39′51″ E; Fig. 2) forms our natural laboratory. To the best of our knowledge, the role of meandering-river oxbow lakes in As-mobilization has been poorly studied. Moreover, none of the studies has taken such an interdisciplinary top-down approach, exploring the terrestrial sources using satellite data, geochemical and microbiological data, and thereafter building a model of *in situ* processes in the abandoned channels of As-affected alluvial plains.

2. Depositional setting

Holocene meandering-river and floodplain deposits of the Ganga River (Fig. 1) form the geomorphology of the alluvial landscape. Sand is transported by the river in suspension in the water column and as bed-load and sediment along the channel floor, and accumulates in point bars on the inner river bends (Fig. 1; Bridge, 2003). The floodplain bordering the river is inundated in the yearly monsoon periods and accumulates silt and clay sediment that settles out of suspension from the floodwaters. During the monsoon periods from May through September, the south-westerly winds with the intensity of ~11.5–28.0 m/s predominate, along with peak discharge of river Ganges as high as up to 75,000 m³/s (FAO, 2015). This may lead to Ganga Brahmaputra river sediment contribution of 700 Mt/yr to ~15 Gt/yr (Dietrich et al., 2020) of the global sediment budget. Due to differential compaction, the sand-prone point-bars stand out as a positive relief in the flat clayey floodplain landscape (Sahu and Saha, 2015). Communities are preferentially located on the point bars because their elevated position is a protection against seasonal river flooding (Fig. Graphical abstract). Direct hand-pump groundwater extraction for consumption and irrigation occurs from the porous and permeable point-bar sands (Donselaar et al., 2017). Crescent-shaped oxbow lakes occur scattered in the alluvial landscape (Fig. 1B).

3. Methods

3.1. Sampling strategies

Suhiya oxbow lake, located on the alluvial plain of the Ganga River in Bhojpur District, Bihar, India (Figs. 1, 2), was selected as natural laboratory for this study. The geomorphology of Suhiya oxbow lake shows its chute-channel cut-off origin (Fig. 1B, C). The main village (Suhiya) on the southern bank of the oxbow lake has a poorly-constructed sewage system that drains directly into the lake (Fig. 2C). The southern part features a regular agitation and mixing
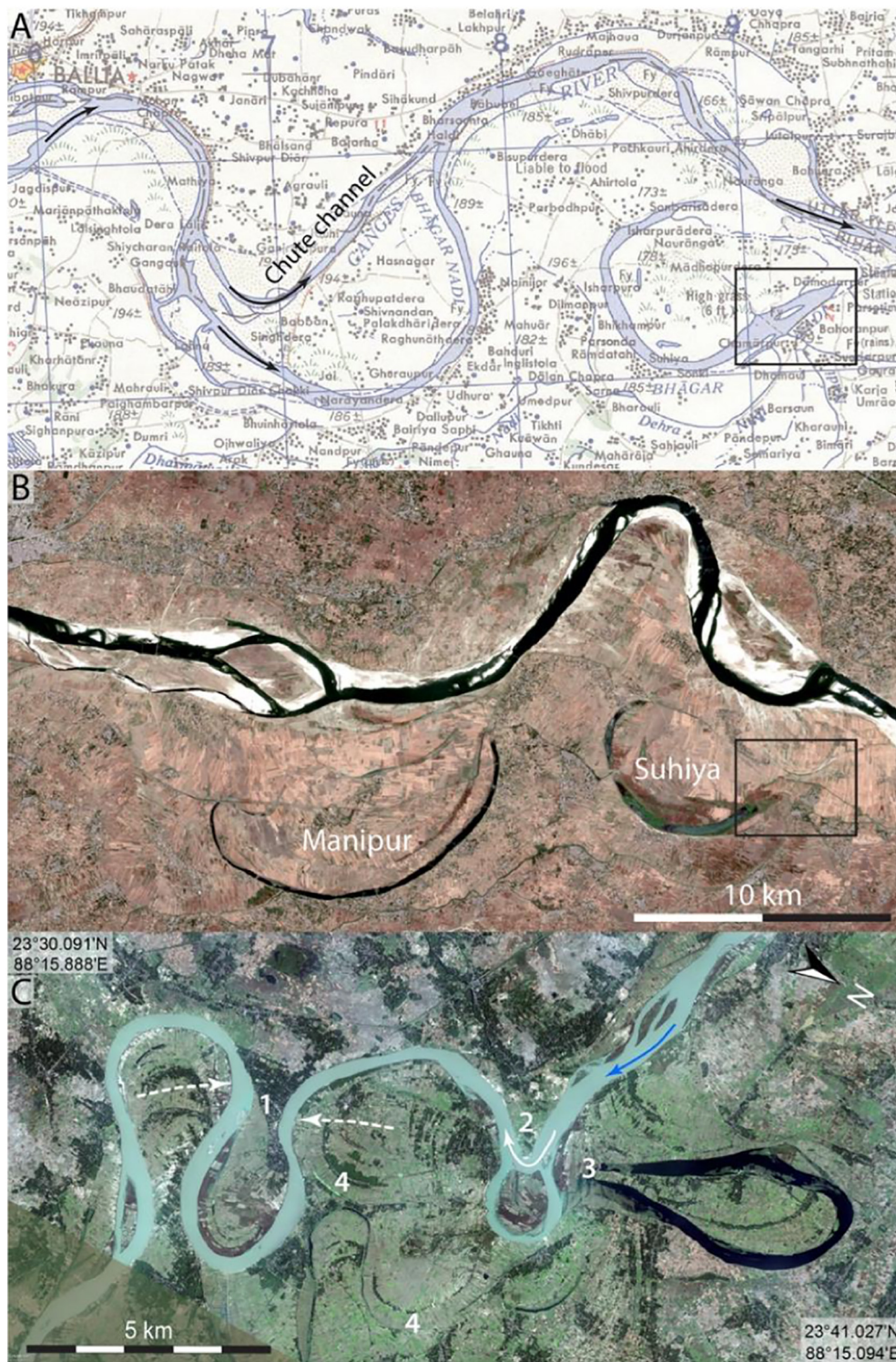
Fig. 1. Evolution of Manipur and Suhiya oxbow lakes over time along the course of the Ganga River. A: Topographical map, compiled in 1955 by US Army Corps of Engineers from Half-Inch Series, 1:126,720, Survey of India, 1931–1938, B: Google Earth-Pro image, 2020-04-10. Black box: Reduction in Suhiya oxbow lake area between 1931 and 1938 and 2020 by lacustrine delta progradation. Arrows: flow direction of the Ganga River, C: Different stages of meander-loop neck cut-off of the Ganga River (West Bengal, India). River flows to the southeast (blue arrow). (*1*): Opposite outer river bend approach (dashed arrows) by cut-bank erosion. (*2*): Neck cut-off (solid arrow) in full progress; longer meander loop still part of the active river. (*3*): Completed neck cut-off; meander loop converted to oxbow lake. (*4*): Oxbow lake completely sediment-filled and converted to clay plug. Google Earth-Pro image, 2010-11-30.

of the lake water due to human activity (Fig. 2D). The lake was subdivided into three sampling stations: the south station (S), the central station (C), and the north station (N) near the levee, where the water depth is maximum (Fig. 2). Water samples were collected in sterile vials for various downstream analyses, from the surface and near bottom of each stations and henceforth the samples are referred as north surface (NS), north bottom (NB), central surface (CS), central bottom (CB) south surface (SS) and south bottom (SB). The physicochemical parameters (temperature and pH) were measured *in situ*.
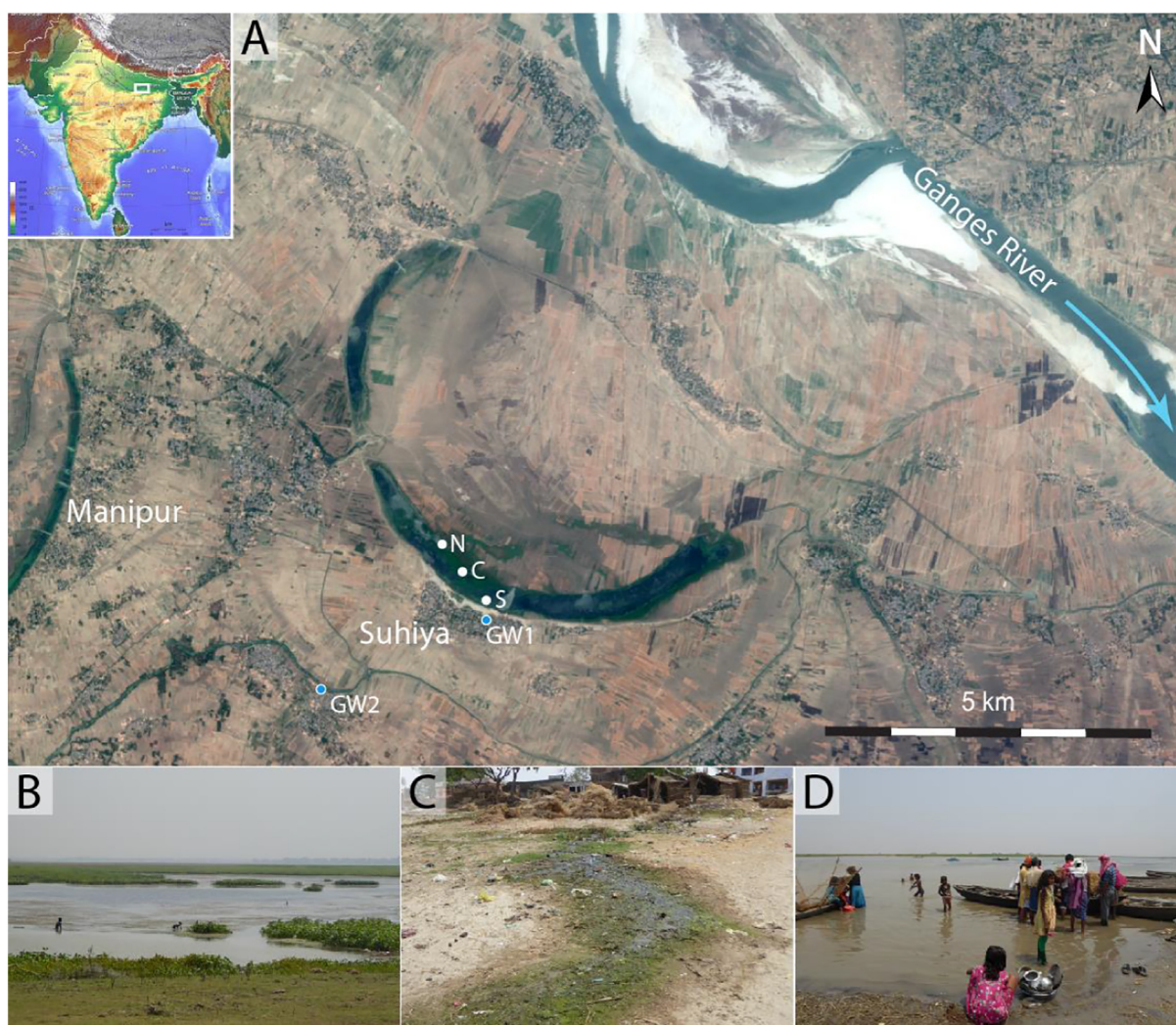
Fig. 2. Sampling locations. A: Google Earth-Pro image of Suhiya oxbow lake, indicating the sampling stations: South (S), Central (C) and North (N), and the groundwater well locations (GW1 and GW2). Blue arrow: flow direction Ganga River. B: High proliferation of *Hydrilla sp.*. C: Open sewage disposal at the southern bank, D: Other human activities (anthropogenic input) and mixing of water at the southern bank.

A long core of 16 m (SHY-1; Fig. 5D) and a short core of 30 cm (SHY-2) were retrieved from the lake bottom. Six subsamples were extracted from SHY-1 and were dried and homogenized before further analysis. The core SHY-2 was centrifuged at 6000 rpm for 20 min and ~2.58 ml of pore water was collected and is henceforth referred as PW. The core was further divided into top sample (0–5 cm as SHY2–5) and bottom (5–10 cm as SHY2–10). Groundwater samples were collected from two borewells (2 samples; GW1, GW2) in the village Suhiya. The lake vegetation was sampled for taxonomic identification.

3.2. Inorganic chemistry analyses

All the water samples (lake water, pore water and groundwater) were collected in triplicate from three sites at surface and bottom, and were filtered through 0.45 μm after acidification. The samples were diluted up to 100 times before analysis. For the sediment samples (6 from core SHY1 and 2 from core SHY2) elemental extraction using 7 M HNO_3 at 100 kPa and 121 °C for 30 min was performed following Swedish Standard Method (SIS, 1993). The certified standard reference sediment CRM-601 was used. All the water samples and sediment samples digests were quantified on an inductively coupled mass spectrometer (ICP-MS-Thermo Scientific X-Series II). Internal standard (Yttrium, for instrumental drift), elemental solution standards and certified

reference water (Environment Canada waters TMDA-64.2) were run with each, 10 and 15th sample respectively.

3.3. Organic chemistry analyses

3.3.1. Characterization of low molecular weight (LMW) molecules

3.3.1.1. Dissolved Organic Carbon (DOC) and aromatics. All the water samples were stored at 4 °C and shipped to laboratory to detect the DIC, DOC (Shimadzu TOC-V CSH analyser), UV_{254} (Agilent Cary Eclipse) and Specific ultraviolet absorbance (SUVA) analysis. Specific UV absorbance ($SUVA_{254}$) (l/mg·m) was calculated as a ratio of UV_{254} (l/m): DOC (mg/l). Potassium Hydrogen Biphthalate (KHP) was used to calibrate the spectrophotometer (APHA), with a spike of $NaNO_3$ (concentration range 0–100 mg/l) and $FeCl_3 \cdot 6H_2O$ (concentration range 0–3.5 mg/l), to determine the effects of nitrate and ferric iron on absorbance.

The stable carbon isotope ratio ($\delta^{13}C_{DIC}$) of DIC was measured following Assayag et al. (2006) and Ader et al. (2006). The ^{12}C and ^{13}C isotopes were analysed on an Isotope Ratio Mass Spectrometer (IRMS) coupled to Gasbench II (Finnigan MAT Delta Plus XL, Germany) with a CTC PAL-80 autosampler. The stable carbon isotope ratio is reported in the delta notation that expresses $^{13}C/^{12}C$ ratios as $\delta^{13}C$ values [per mil (‰); Eq. (1)] in relation to the reference standard Vienna Pee Dee Belemnite (V-PDB):

$$\delta^{13}C = \left[\frac{\left(^{13}C/^{12}C_{sample}\right)}{^{13}C/^{12}C_{reference}}\right] \times 100 \qquad (1)$$

$$Bacterial\ DOC\ (\%) = \left[\frac{\sum d_{AABI}}{\sum d_{AABI}}\right] \times 100 \qquad (2)$$

where, Σd_{AABI} is the total d-amino acids (Asx, Glx, Ser, Ala) in water samples before incubation and Σd_{AAAI} is the total d-amino acids (Asx, Glx, Ser, Ala) in water samples after incubation.

3.3.1.2. Characterization of amino acids. All the samples from the bioassay experimental sets were filtered through 0.2 μm filter before analysis. The amino acid enantiomers were derivatized using o-phthaldialdehyde and N-isobutyryl-L-cysteine and were separated on Agilent Poroshell 120 EC-C18 column in an Agilent 1200 high-performance liquid chromatography system equipped with a fluorescence detector (LCFD). The LCFD data of the eleven amino acids were normalized with the DOC values and reported as Total Dissolved Amino Acids (TDAA; Fig. 3).

3.3.1.3. Amino acid proxies as microbial contributions to DOC. Microcosm based experiment: Lake water samples (surface and bottom) were collected to estimate microbial contribution to LMW-DOM. In this experiment the waters samples were filtered through pre-combusted filters (pore-size 0.7 μm; Whatman) to remove particulate matter and eukaryotic cells. These water samples (100 ml) were then incubated in at 25 °C in aphotic conditions for 21 days. Microbial contributions to groundwater DOC were estimated using d-amino acids as tracers of bacterial carbon (Eq. (2); Kawasaki and Benner, 2006). The fraction of bacterially-derived DOC was calculated as:
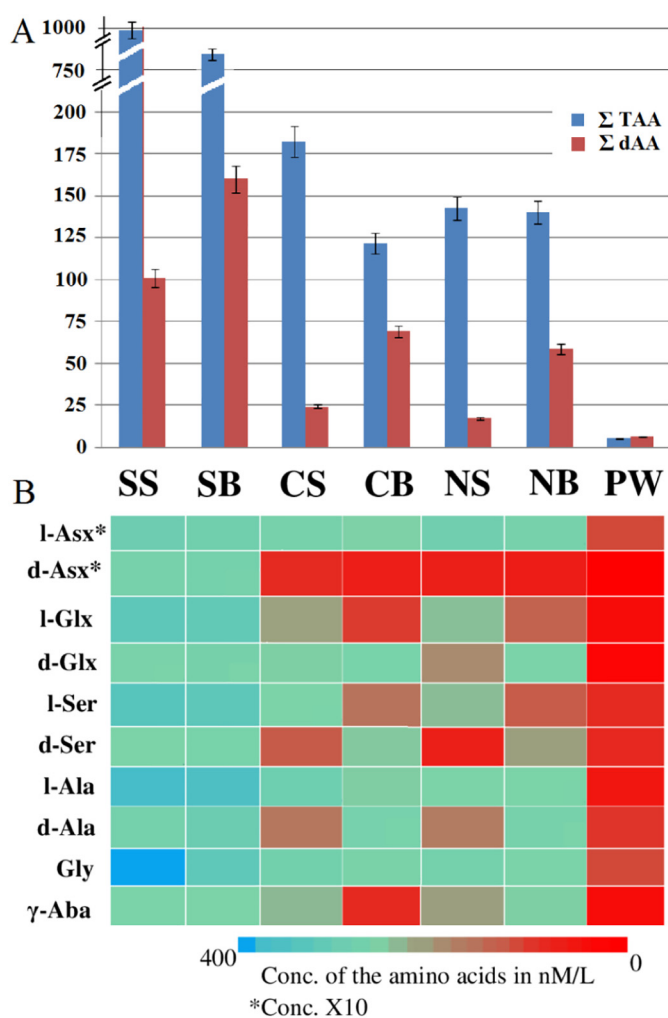

Fig. 3. A: Abundance of total dissolved amino acids (TDAA) and total d-enantiomer of the amino acids (dAA); B: The heat map depicts the distribution of each enantiomer of the amino acid across the lake. [*Conc. is 10X].

3.3.2. Characterization of high molecular weight (HMW)-DOM

3.3.2.1. Lignins and phenols. Lignin phenols were analysed in surface and bottom samples in duplicates to trace plant-derived molecules in the DOM. About 2 l of water samples were filtered through 0.2 μ filters (Millipore) and were acidified to pH 2.5 using suprapure sulfuric acid (Merck) and were extracted using C-18 cartridges (Sigma Bond Elut®; Louchouarn et al., 2000). The lignins were eluted with methanol (30 ml) and detected by CuO oxidation method (Kaiser and Benner, 2012).

The oxidized forms of lignin were quantified in an Agilent 7890 gas chromatograph with a DB5-MS capillary column and an Agilent 5975 mass selective detector. Six lignin phenols were measured: vanillin (VAL), acetovanillone (VON), vanillic acids (VAD), syringaldehyde (SAL), acetosyringone (SON), syringic acid (SAD), further reported as total dissolved lignin phenols (TDLP$_6$). The data was normalized with the DOC values.

3.3.2.2. Alkane hydrocarbons. To characterize *n*-alkanes, 2 l water samples were filtered through the ENVI^{TM} C-18 SPE DSK (C-18 bonded silica; Sigma–Aldrich) discs. To pre-condition the discs, 5 ml of methanol (MeOH) and 5 ml de-ionized water were passed. The discs were stored at 4 °C and carried to laboratory where they were lyophilized (Labconco), weighed and stored in the refrigerator (4 °C) until further processing. The lipid fractions were extracted using dichloromethane (DCM) and methanol mixture (9:1 v/v) using ultrasonication (Wu et al., 2014) and quantified (GC–MS parameters) as per Ghosh et al. (2015a).

3.3.3. Sedimentary organic carbon (SOC) characterization

The TOC% of the six sediment samples of core SHY-1 were measured following Sutherland (1998), and for core SHY-2, the TOC% and TN% in core samples SHY2-5 and SHY2-10 were measured in a LECO truspec CN analyser. The complex long chain sedimentary hydrocarbon deposition was detected by analysing ~1 g of freeze-dried and homogenized sediment samples (SHY2-5 and SHY2-10) were used for ultrasonication based lipid extraction in DCM: methanol (9:1; Wu et al., 2014) and processed as per Ghosh et al. (2015b). The lipids were quantified using above mention GCMS parameters.

3.4. Microbiological analyses

3.4.1. Identifying the key microbes

To identify the key microbial players in contributing to DOM, 100 μl of each the six water samples were used as inoculum to grow the strains in four BG11 agar media (Hi Media; pH 7) each, supplemented with glucose (250 μM/l). The BG11 agar plates were incubated in at 25 °C (Avg. annual Suhiya lake-water temp.) for 48 h. About 45 to 50 different colonies were isolated from each sample set. Un-supplemented (without C-source) BG11 liquid enrichment culture were prepared and later grown on a set of three un-supplemented BG11 agar plates per water sample, at 25 °C in photic conditions to study autotrophic bacterial groups (*Cyanobacteria*). A total of 416 bacterial strains were isolated and the molecular characterization was done.

Genomic DNA of each of the strains were extracted using DNeasy Power Lyzer Microbial Kit (Qiagen) and the polymerase chain reaction (PCR) amplification of its partial 16S rDNA was done using eubacterial primers Fc27 (5′-AGA GTT TGA TCC TGG CTC AG-3′) and Rc1492 (5′-TAC GGC TAC CTT GTT ACG ACT T-3′; Lane, 1991). The detail of PCR

reaction cocktail and amplification conditions are described in Chikkanna et al. (2018). The cyanobacterial genomic DNA extracts were used as template with the cyanobacteria specific 16S rRNA gene primers CYA106F (5′-CGG ACG GGT GAG TAA CGC GTG A-3′), and CYA781R (5′-GAC TAC AGG GGT ATC TAA TCC CTT T-3′), following the PCR conditions in Nübel et al. (1997). The 416 PCR products were purified using QIA quick PCR Purification Kit (Qiagen) and sequenced using the same primers in an ABI Prism 3730 Genetic Analyzer based on Big Dye Terminator chemistry (Applied Biosystems, California, United States). All the sequences are available in GenBank (accession no. MW383510 to MW383925). The phylogenetic representation of with an unrooted tree for the identified strains was done using Neighbour Joining method based on JTT Model (Jones et al., 1992) was used to construct the phylogenetic tree for aioA in MEGA version 10.0 (X) (Stecher et al., 2020).

3.4.2. MPN test for coliform detection

To detect the coliform load in the water samples a classic method of Most probable Number (MPN) test (Oblinger et al., 1975), was adopted using Mac Conkey broth with Bromo cresol purple (5′, 5″-dibromo-o-cresol sulfophthalein) dye (Hi Media) with Duhram's tube inserts.

3.5. Remote-sensing based time-series image analysis of macrophytes

The work hypothesis in the present study is that macrophyte vegetation has a large impact on As-fluxes. Remote-sensing imagery was used for the analysis of the vegetation dynamics and the evolution throughout the year of the macrophyte density in the oxbow lake. For this remote sensing study, Sentinel-2 satellite image data were analysed of a complete calendar year with one image of per month (Sahai et al., 1985; Chari et al., 1994; Jonna et al., 1995). The images were analysed in ArcGIS (Ray et al., 2002) for growth pattern and calculation of the total surface area of the oxbow lake covered with vegetation and without. Cloud-free data were not available in the monsoon months July to September 2019; the data gap was filled with images from the previous year, 2018. Four out of twelve available multispectral bands [Blue: wavelength 0.490 μm; Green: 0.560 μm; Red: 0.665 μm and NIR (Near Infrared): 0.842 μm] were layer-stacked to a single image with 10 m spatial resolution, from which the macrophytes surface area was quantified. Unsupervised classification technique and maximum likelihood algorithm were used to analyse the multi-band layer stacked Sentinel-2 image. Gradual changes in the reflectance values of the water surface were interpreted as the growth of the vegetation (Sahai et al., 1985; Chari et al., 1994; Jonna et al., 1995; Navalgund et al., 2007; Ray et al., 2015). Usually, in a RADARSAT SAR analysis, data collected over a period of every 25 days temporal resolution are used to assess crop parameters such as plant height, age and plant biomass (Ribbes and Le Toan, 1999; Chakraborty et al., 2005). Also, microwave remote sensing technique could be used, based on the measurement of dielectric signal differences generated due to the reflectance of open water surface relative to that of vegetation. It is generally used for the estimation of the growth of floating vegetation such as Eichhornia sp. (Costa, 2004; Evans et al., 2010), but due to lack of wave penetration into the water, it is incapable of quantifying the growth of submerged plant bodies such as Hydrilla sp. Hence, we preferred the use of optical data of every 25 days for this study. The layer-stacked Sentinel-2 satellite images of a year were used to generate a video file for visualizing the chronological changes in the oxbow lake vegetation coverage throughout the year (Video 1). The remote sensing analysis was complemented with ground-truth observation of the vegetation type and density during fieldwork campaigns in January 2013, April 2016, and April–May 2018.

3.6. Side-scan sonar survey and sediment coring

Three side-scan sonar surveys across the Ganga River, Manipur and Suhiya oxbow lakes served to generate the cross-sectional river-depth

profiles. In combination with the analysis of vintage topographic maps from 1931 to 1938 (map by US Army Corps of Engineers, 1955; Fig. 1A), present-day Google Earth-Pro imagery, and a sediment core in the bottom of Suhiya oxbow lake (Figs. 1, 5), quantifications were made of the sedimentation rate, and the reduction in oxbow-lake surface area and river-depth after channel abandonment.

4. Results

4.1. Elemental distribution

The water samples from the surface (NS, CS and SS) had higher overall elemental concentration than the bottom water samples (NB, CB and SB) < GW < PW (Table S1). The drastic reduction on the surface could be due to adsorption by the macrophytes (Ghosh and Biswas, 2015). The water samples from south bank showed abundance of elements such as Cd and Pb (Table S1). The As concentration in the water samples was relatively lower than in the PW and adjacent groundwater samples (Fig. 4). The elemental concentration in sediments showed a similar trend such as water with abundance of Cd and Pb in south bank (Table S1). The sedimentary As concentration was higher in the top layers and eventually reduced, and had a direct correlation with the organic content of the sample (Fig. 5D).

4.2. Distribution of organic molecules

The DOC values of lake water ranged from 674 to 1538%, and were higher in the bottom water samples. The average $\delta^{13}C$ value of the water samples was −23‰ and average $\delta^{15}N$ was 4.13‰ (Fig. 6A). The lake bed sediment samples had an average TOC value of 0.8%. To understand the distribution and bio-availability of organic molecules to the DOC molecules were separated based on their size and hydrophobicity.

4.2.1. Hydrophilic labile groups

The predominance of aromatics with high SUVA$_{254}$ in the surface samples was observed in comparison to the bottom-water and pore water samples. The surface-water sample SS had the highest aromatic
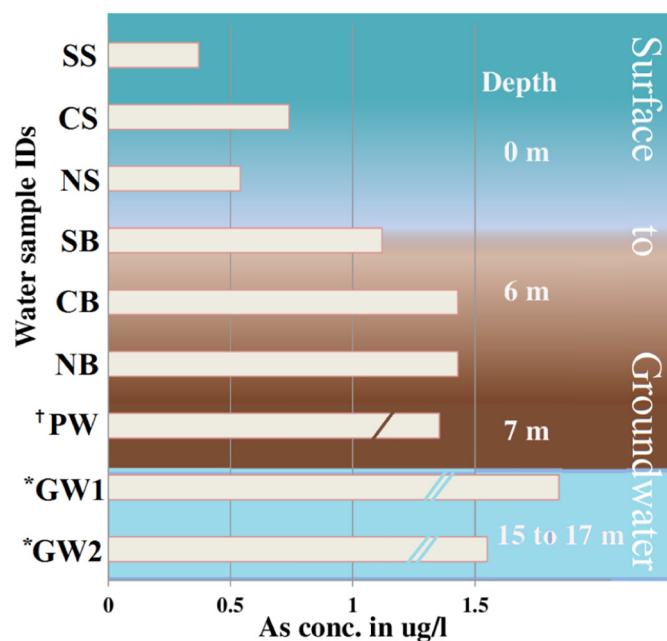
Fig. 4. Distribution of arsenic across the oxbow lake channel, indicating role of the clay plug in mobilization and spike of As in groundwater relative to the surface water. [*Conc. is ×100, †Conc. is ×10].
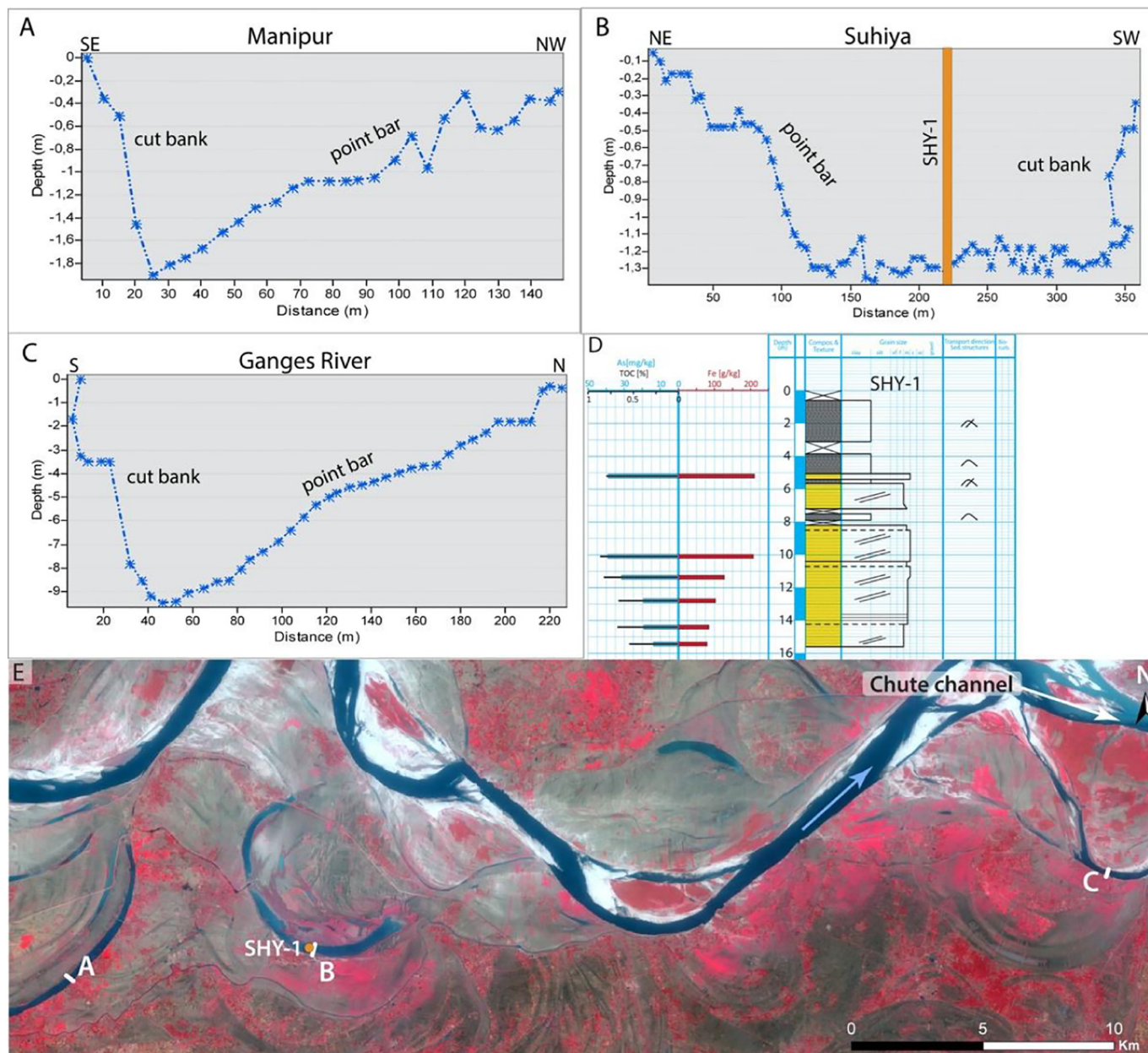
Fig. 5. A–C: Side-scan sonar profiles, D: Sedimentological core-description log SHY-1, Suhiya oxbow lake. The As (g/kg) and Fe (g/kg) plots are the results of elemental analysis vs TOC% of the core samples, E: location of profiles A-C and borehole SHY-1. Blue arrow: flow direction of the Ganga River.

load (4.6), relative to CS (3.49) and SS (2.62), and was very low (0.42) in PW (Fig. 6B).

Among the amino acids, both the enantiomers (d and l) of all the measured amino acid decreased in the bottom waters compared to the surface. After the incubation period, a 15 to 23% decrease was observed in TDAA the water samples. The d-enantiomers of the amino acids $\sum$dAA (Fig. 3A) were used as proxies to calculate microbial contribution: *Bacterial DOC%*, which varied from 13 to 29.5% of the total DOC.

4.2.2. Hydrophilic less-labile groups

The surface water samples had high dissolved lignin load. The TDLP$_6$ values ranged from 922 to 2854 nmol/l in the lake water samples, and showed a good correlation with a$_{254}$ (Fig. 6C), except for sample SS remained as an outlier.

4.2.3. Hydrophobic groups

The total *n*-alkane abundance in the samples varied from 273 to 2764 ng/l. The SS samples showed a bimodal distribution with predominance of both short chain *n*-alkanes (C$_{13}$ to C$_{21}$) and long chain (C$_{23}$ to C$_{35}$). A predominant abundance of *n*-C$_{22}$ was observed in all surface samples. To predict the sources of these hydrocarbons, various ratios were used. Modified Carbon Preference Indexes (CPI) for aquatic systems predicted by Ghosh et al. (2015a) as CPI$_{TOT}$ (*n*-C$_{13}$ to *n*-C$_{35}$), CPI$_{LMW}$ (*n*-C$_{13}$ to *n*-C$_{21}$) and CPI$_{HMW}$ (*n*-C$_{23}$ to *n*-C$_{35}$) [Eqs. (3) to (5); Fig. 6F]. The CPI$_{TOT}$ (ranged from 2.07 to 8.55) and CPI$_{HMW}$ (ranged from 3.13 to 24.09) were higher in the bottom water from all the sites, whereas CPI$_{LMW}$ (ranged from 1.68 to 15.84) was high in surface water.

$$CPI_{TOT} = \frac{\sum (C_{13} \text{ to } C_{33})_{odd} + \sum (C_{15} \text{ to } C_{35})_{odd}}{2\sum (C_{14} \text{ to } C_{34})_{even}} \quad (3)$$
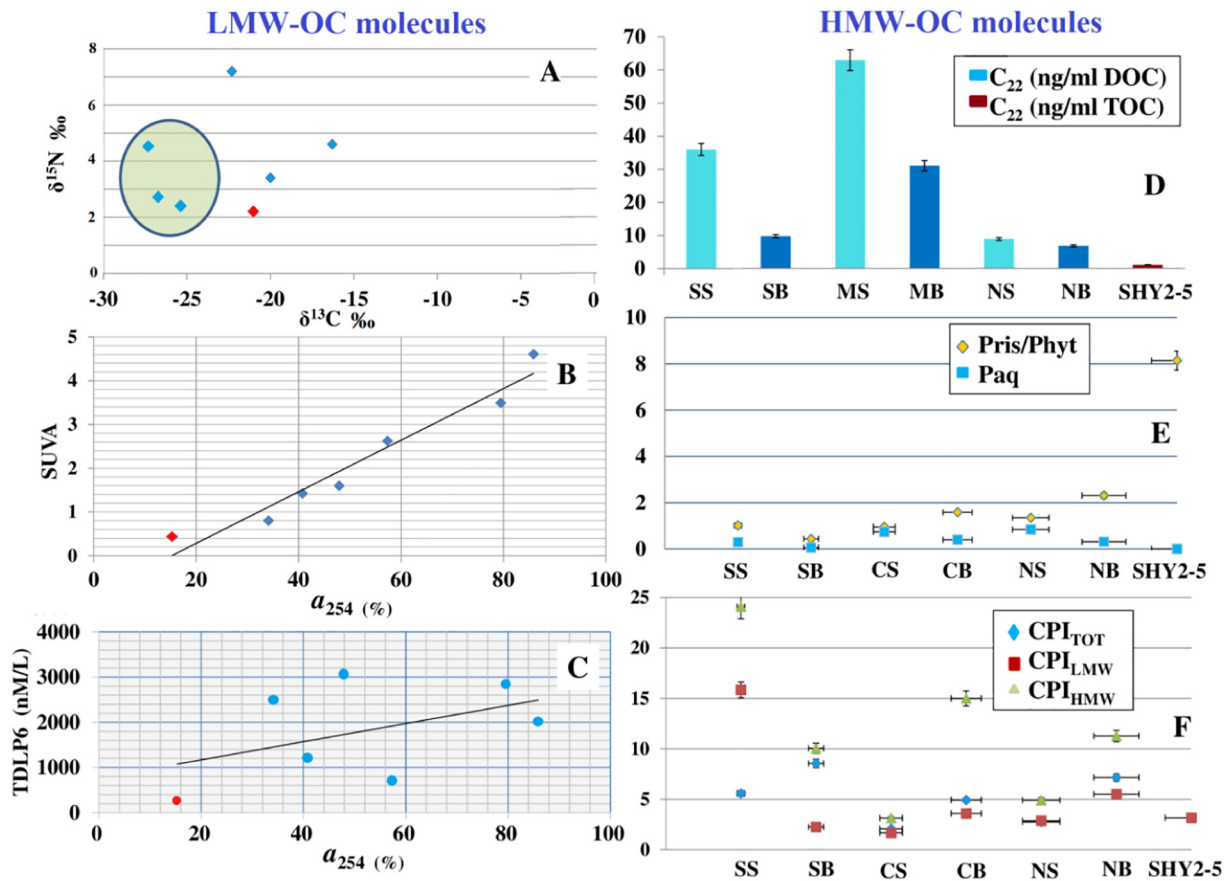
Fig. 6. Characterization of OC molecules. A: The $\delta^{13}C$ vs $\delta^{15}N$ values of the water samples. The lower values in the surface samples highlighted by the circle indicates macrophyte respirations. The red dot represents the PW sample, with low $\delta^{15}N$. B: The absorption at 254 vs SUVA value indicates a liner regression. C: The absorption at 254 vs Total dissolved lignins-phenols. D: The distribution of n-alkane C_{22} in the water and sediment samples, indicating predominance of C4 respiration in the surface. E: The low molecular weight (LMW), high molecular weight (HMW) and total Carbon Preference Index (CPI) of the n-alkanes in water and sediment.

$$CPI_{LMW} = \frac{\sum (C_{13} \text{ to } C_{19})_{odd} + \sum (C_{15} \text{ to } C_{21})_{odd}}{2 \sum (C_{14} \text{ to } C_{20})_{even}} \quad (4)$$

$$CPI_{HMW} = \frac{\sum (C_{23} \text{ to } C_{33})_{odd} + \sum (C_{25} \text{ to } C_{35})_{odd}}{2 \sum (C_{24} \text{ to } C_{34})_{even}} \quad (5)$$

Modified Average Chain Length (ACL; Cranwell et al., 1987; Ghosh et al., 2015a; Eq. (6)) was used to interpret the distribution/abundance of predominant n-alkanes in DOC and SOC. The ACL varied from 27 to 31 indicated the predominance of terrestrial sources such as angiosperms. The Paq ratio (Eq. (7)) was calculated to range from 0.05 to 0.83, indicating OC input from sources such as submerged/floating aquatic macrophytes (Zhang et al., 2004).

$$ACL = \frac{\sum (nC_n \text{ to } mC_m)_{odd}}{\sum (C_n \text{ to } C_m)_{odd}} \quad (6)$$

where, n (lowest C-number) = 15 and m (highest C-number) = 33

$$Paq = \frac{C_{23} + C_{25}}{C_{23} + C_{25} + C_{27} + C_{29}} \quad (7)$$

A ratio of quantified-abundance of the isoprenoid-alkanes Pristane and its derivative Phytane was used as a redox indicator (Rontani and Volkman, 2003; Ghosh et al., 2017). The southern bank samples SS and SB (1.01 and 0.43 respectively) had low Pristane/Phytane, and was high in NB (2.3) and highest in PW (8.14; Fig. 6E).

4.3. Microbial cell size, abundance and metabolism

The major bacterial classes identified were *Betaproteobacteria*, *Gammaproteobacteria*, *Bacilli*, *Actinobacteria* and *Cyanophyceae* (Fig. S2). The bacterial community dynamics based of 16S rRNA molecular diversity in the six lake water samples displays different diversity patterns (Fig. 7). The surface water sample NS and CS were dominated by bacterial genera with larger size (10 to 25 μm) and lower cell surface area (SA): volume ratio like *Microcystis* and *Nostoc*, and *Burkholderia*, while the *Cyanophyceae* abundance decreases in the bottom. Towards the south both SS and SB has Enterobacterial dominance along with *Burkholderia*. Other than these, all samples had bacterial genera with smaller cell size (0.5 to 2 μm) and higher cell SA: volume ratio such as *Acinetobacter*, *Hydrogenophaga*, *Acidovorax*, *Aquimonas*, *Pseudomonas*, *Bacillus*, *Nitrosomonas* and *Decholomonas* which were reported to be involved in microbial As-cycling and or linked metabolic pathways (Ghosh et al., 2014).

The abundance of coliforms was confirmed by the MPN test results. The coliform DNA signatures were only found in samples SS and SB (both had MPN 14 per 100), and faintly in CS (MPN- 2 per 100; Table S2).

4.4. Remote sensing-based time series analysis of the oxbow lake

The Sentinel-2 image analysis showed that monsoonal flooding (August–October) resulted in the sharp decline of reflectance values (Fig. 8D). The low post-flood macrophytes coverage area (Fig. S1)
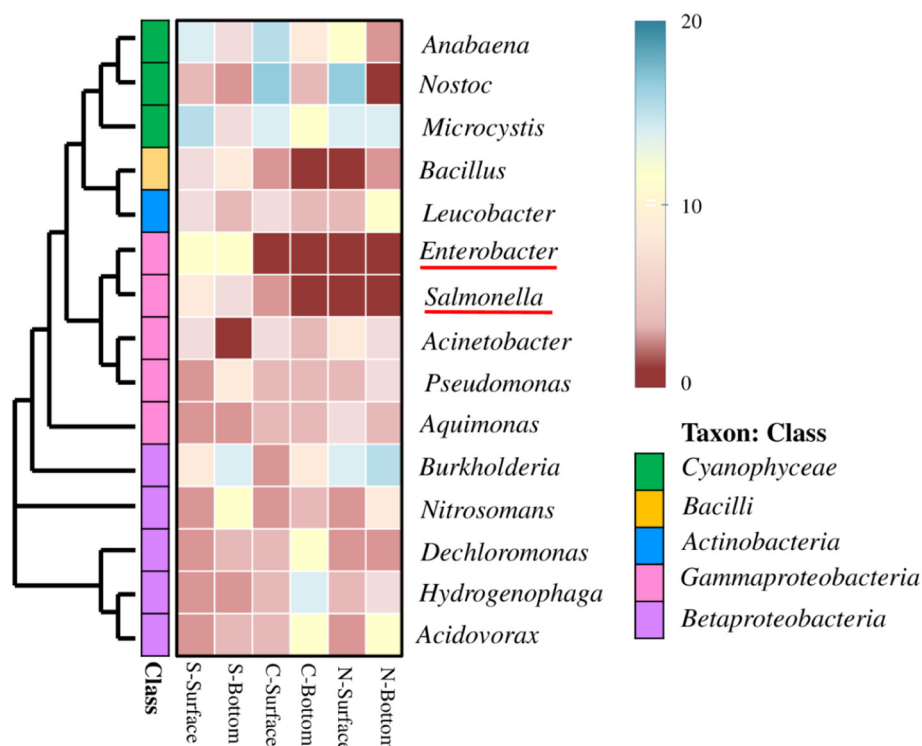
Fig. 7. Distribution and abundance of bacterial genera. The samples SS and SB indicates predominance of the family *Enterobacteriaceae* (*Enterobacter* sp. and *Salmonella* sp.). The genera from family *Cyanophyceae* are marked in green shades, shows predominance in surface samples.

suggests that the macrophytes are largely eradicated during the flood period, and start reoccupying the lake waters from November onward, to reach their peak density in June, when the macrophytes cover up to 3.91 km^2, or 89% of the total oxbow-lake surface of 4.37 km^2 (Table S4). The Sentinel – 2 images from November to July were classified to quantify/calculate the area covered with macrophytes (Table – S4), and were further overlaid on their corresponding satellite images to present/visualize the result (Fig. S3/Video 2). Due to flooding from August to October, the classified Sentinel-2 satellite data do not show any vegetation, and were therefore not included in Fig. S3/Video 2.

5. Discussion

The Suhiya oxbow lake long-core SHY-1 (Fig. 5D) comprises an 8.2 m thick succession of dark-grey clay with shell debris and a distinct H$_2$S smell. This interval represents the partial suspension-load fill of the clay plug. The cross-stratified fine-grained sand at 5.8 to 7.2 m is the preserved bed-load dune deposit on the channel floor that formed in the active river phase prior to chute cut-off (Donselaar and Overeem, 2008). The cross-stratified, fine- to medium-grained sand layers in the lower half (Fig. 5D, 8.2 to 15.6 m) are point-bar deposits from an older phase of the Ganga River.

Side-scan sonar profiles across the studied oxbow lakes and the present-day Ganga River (Fig. 5A to C), in combination with the SHY-1 core data, allowed for the estimation of the sediment infill rate of the oxbow lakes. The location of the Ganga River profile (Fig. 5C) is chosen for its similarity with the Manipur situation in 1931–1938 (map by US Army Corps of Engineers, 1955; Fig. 1A). The river section is still active in both, but part of the flow is diverted in a chute channel (Fig. 5D). The assumption is that in its active phase the maximum depth of Ganga River does not vary along the 85 km graded river stretch between Manipur and the Ganga River profile location. The assumption is supported by the sedimentology in the SHY-1 borehole, where the sum of the clay-plug thickness (8.2 m) and the oxbow-lake water depth (1.3 m, Fig. 5B) equals the 9.5 m water depth in the Ganga River profile

(Fig. 5C; Kumar et al., submitted). The water depth in the Manipur profile (Fig. 5A) is 1.9 m, which means that the reduction of 7.6 m from the original depth of 9.5 m is accounted for by suspension-load sediment aggradation after the chute-channel cut-off was completed, somewhere after the year 1938, and until 2017, when the side-scan profile was shot. The resultant minimum sedimentation rate (760 cm in 79 yr) is 9.6 cm/yr, whereby clay compaction is not taken into account. Extrapolated to the Suhiya oxbow lake, with clay-plug thickness of 8.2 m, the sediment-accumulation time since chute-channel cut-off would be 85 yr. The 2 km progradation of a lacustrine delta in the NE end of Suhiya oxbow-lake (black boxes in Fig. 1A, B) has contributed to the reduction of the total lake volume.

Presence of young DOC at depths in excess of 80 m in Bengali groundwaters demonstrates that DOC must be transported to greater depths along flow paths that are likely to be significantly impacted by the extensive groundwater pumping that prevails in this region. The high DOC vs low δ^{13}C values usually indicate the source to lie between marine and freshwater environments (Nowak et al., 2017), however, such values from our samples are due to the terrestrial runoff and the shift from C$_4$ to C$_3$ respiration in the dominant water plat *Hydrilla* sp. As an effect of the As, Cd, Pb and other heavy metals, which reduces the photosynthetic rates in macrophytes (Srivastava et al., 2013; Fletcher et al., 2020).

The elemental analysis detected anthropogenic tracers (such as Cd and Pb) in the south bank (both waters SS and SB and sediment SHY2-5; Bhattacharya et al., 2008). The elevated levels of all elements in the sediment are due to the deposition and adsorption/binding to the organic matters present (Kaiser et al., 2004; Ghosh et al., 2015b). The flooding and river water intrusion into the lake, brings high inorganic load which gets adsorbed and bound to the lake water vegetation mostly by *Hydrilla* sp. and *Eichhornia* sp. (Fig. 2), is the possible source of the organic matter bound elements.

To understand the preservation and bioavailability of LMW OC, the SUVA$_{254}$ representing the aromatic groups present in the DOC were studied (Weishaar et al., 2003). The aromatic molecules and amino
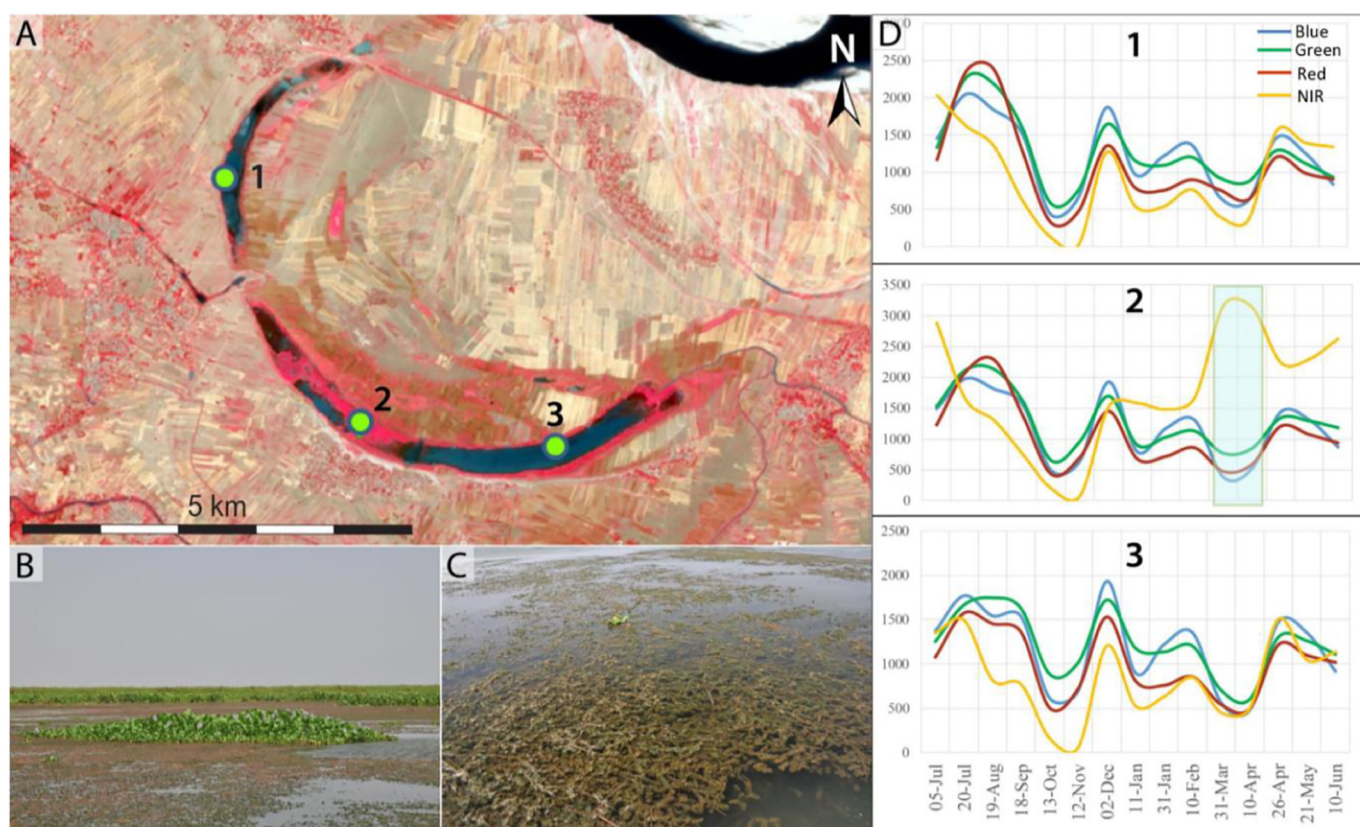
Fig. 8. Reflectance analysis of vegetation cover, Suhiya oxbow lake. A: False-colour Sentinel-2 satellite image (Blue, Green, Red, and NIR (Near Infrared) bands) of the study area. Image date: 10 April 2020. B: *Eichhornia* sp. (above the water surface; light green) and *Hydrilla* sp. (at and below the water surface; reddish-green) macrophytes colonize the oxbow-lake, C: Close-up of *Hydrilla* sp. vegetation. Both photos were taken in Suhiya oxbow lake in April 2018, D: Reflectance variation per month. NIR band indicates the growth development of vegetation over the year. Note the sharp decline in NIR values in the October–November monsoon flooding. Blue = 0.49 μm; Green = 0.56 μm; Red = 0.665 μm, NIR = 0.842 μm. Vertical axis scale: Top of Atmosphere (TOA) reflectance units × 10,000.

acids represent the labile OC i.e., the LMW-DOC (Kaiser and Benner, 2008), and their abundance at surface, suggesting an enrichment of fresh sources (Planktonic biomass) and decline of their abundance in the bottom as indicated by the diagenetic activity and utilization of the bioavailable OC macromolecules by the microbial communities. Moreover, such diagenesis is also observed in the SUVA$_{254}$ value in PW (Fig. 6). In a natural ecosystem, among the amino acids the dextro-enantiomers are produced by prokaryotic habitants. To understand the contribution of the bacterial population in the LMW DOC load, the microcosm based bioassay experiment was setup. A rapid increase in *Bacterial DOC%* (Eq. (2)) and rapid reduction of TDAA indicates high metabolic activity and diagenesis of bioavailable OC in microaerophilic incubation condition. This also suggests that possibly the metabolic rates vary from hypolimnion of a monomictic lake (such as Suhiya lake) to a holomictic or polymictic lake, as a function of high energy and redox conditions.

To understand the role of indigenous microbial population in metabolic processes, digestion of OC, bioweathering of minerals and mobilization of elements, the isolation and characterization was carried out. All the samples had shown a good bacterial diversity, interestingly both the southern samples SS and SB shows a high coliform load in the MPN test (Oblinger and Koburger, 1975). The predominant bacterial groups involved in As-cycling such as: As(III) oxidizers (e.g. *Acidovorax* and *Hydrogenophaga*) and As(V) reducers (e.g. *Acinetobacter*, *Pseudomonas*, *Bacillus* and *Leucobacter*), were found in the all the lake water samples (Fig. 7); suggesting a dynamic As-cycling. The high MPN count (Table S1) in the southern bank was further explained by the presence of the enteric bacteria such as *Enterobacter* and *Salmonella*. The source of these pathogenic strains could be sewage disposal from the Suhiya

village into the lake. An enterobacterial load was also detected in the groundwaters of this region (Annaduzzaman et al., 2018); indicates migration of bacterial communities along the pull in the water column towards the point bars where the borewells are located in the villages (Fig. Graphical abstract).

Anaerobic degradation was detected in the bottom waters by the low abundance of *l*-amino acids and *n*-C$_{22}$, as the R-NH$_3$ amine groups are oxidized into nitrite by *heterotrophic* microorganisms such as *Pseudomonas* and *Nitrospira* (Gnanaprakasam et al., 2017; Ghosh and Bhadury, 2018). A reduction of upto 17.4% of SUVA and 97.9% of *l*-amino acids was observed at the southern station, where metabolic activity is highest. The terrestrial inputs affect and shape the microbial community structure. Such as these waters are rich in nitrate from agricultural runoffs, are influencing the sustainability of the nitrate-dependent Fe(II)- such as *Acidovorax* and *Dechloromonas*, which are also key players in arsenite As(III) oxidation in this region (Ghosh et al., 2014, 2018). Moreover, the fresh water vegetation such as macrophytes enhances heterotrophic bacterial metabolic processes such as denitrification (Preiner et al., 2020). *Burkholderia ferrariae*, has been reported to mineralize and mobilize phosphate (Valverde et al., 2006). The high abundance of the genera can also impact photoautotrophes (Fig. S2) such as the cyanobacterial genera *Microcyctis*, since the cellular As efflux depends on the dissolved phosphorus levels (Yan et al., 2014; Ghosh and Bhadury, 2018). *Microcyctis* shows a consistent abundance in surface as well the bottom waters of the oxbow lake. Whereas the population of large celled microorganisms like *Nostoc* and *Anabaena* alters along the photic zones and hypolimnion conditions (Fig. 7, S2). For every class of molecule, its uptake depends on the total C and N ratio in the microbial cell and the DOM pool in the microsite of the cell. The

cell SA plays an important role in C-mineralization in any system (Kaiser et al., 2014). Interestingly, a decrease in cell size along with depth in the water column was observed (Fig. 9), suggesting increase in C-mineralization/metabolic rates along the depth. The abundance of specific groups alters depending on the redox gradient. Microbial cells with a higher SA to volume ratio, grow faster than microbial cells of larger sizes. The slower growing larger microbes were found on the dynamic part of the lake (water column). These bacterial genera usually have a slow rate of cell division, mostly invest in strengthening structure and production of defensive compounds in order to reimburse for their slow growth rate (K- vs r-strategists; Kaiser et al., 2014). Observations over small temporal scale suggest with increase in C:N ratio and LMW DOM, microbial biomass increases by utilizing the easy to mineralize C-sources. This may also increase a subsequent abundance of microbial-necromass degraders with very small cell size (Kaiser et al., 2014).

The high lignin and n-C_{22} load in the water samples points to the direct OC input from the water plants *Hydrilla* sp. and *Eichhornia* sp. (Fig. 6C, D). The correlation of $TDLP_6$ with a_{254} suggests the source of aromatic molecules such as quinones and hydroquinones and lignin phenols are closely related/identical (Spencer et al., 2010). Sample SS is an outlier (Fig. 6C) indicating main source of the highly abundant aromatics and aliphatics are terrestrial (ACL indicating angiosperms) or anthropogenic (bimodal distribution). Since lignins are hydrophobic macromolecules, they are readily adsorbed on clay minerals and retained in the lake bed for longer period (Kaiser et al., 2004). Moreover, phytol a chlorophyll constituent forms Pristane which further diagenetically alters into Phytane. The ratio Pristane/Phytane (Fig. 6E) is a key

indicator of redox conditions on such depositional environments, was used as a proxy (Rontani and Volkman, 2003). In clay rich samples such as NB and PW, the kaolinite catalyses the degradation of a plant derived (mostly macrophytic and terrestrial) R-CH_2OH hydrocarbon Phytol, results in increase in abundance of Pristane (R-CH_3) in reducing condition. In a holomictic lake such as the studied one, where there is a thermal stratification, and hypolimnion in the bottom, redox environments facilitates preferential preservation of HMW-OC as indicated by CPI values in CB, NB and PW (Fig. 6F).

Among the dominant macrophytes found in this lake system, *Hydrilla* has a life span of more than two years, (Carter et al., 1994), whereas *Eichhornia* can survive a maximum of four weeks at or above temperatures of 34 °C (Ghosh and Biswas, 2015). The macrophyte growth cycle of the oxbow lake vegetation was monitored with satellite imagery from summer 2019 to summer 2020. It is observed that during the monsoon, flooding of river channel caused eradication of lake-macrophytes, especially *Eichhornia* sp. results in a sharp decline in the reflectance (Fig. 8D). The annual vegetation growth could be seen through the reflectance value shown in the graph data of the post-flood condition in the video (Video 1). The peak of the reflectance during the month March–April is due to reduction in water levels and increase in visibility of submerged growth.

5.1. Oxbow lake - Chromatographic model

The conceptual model was developed to understand the dynamic interplay of the organic matters accumulating from multiple sources into
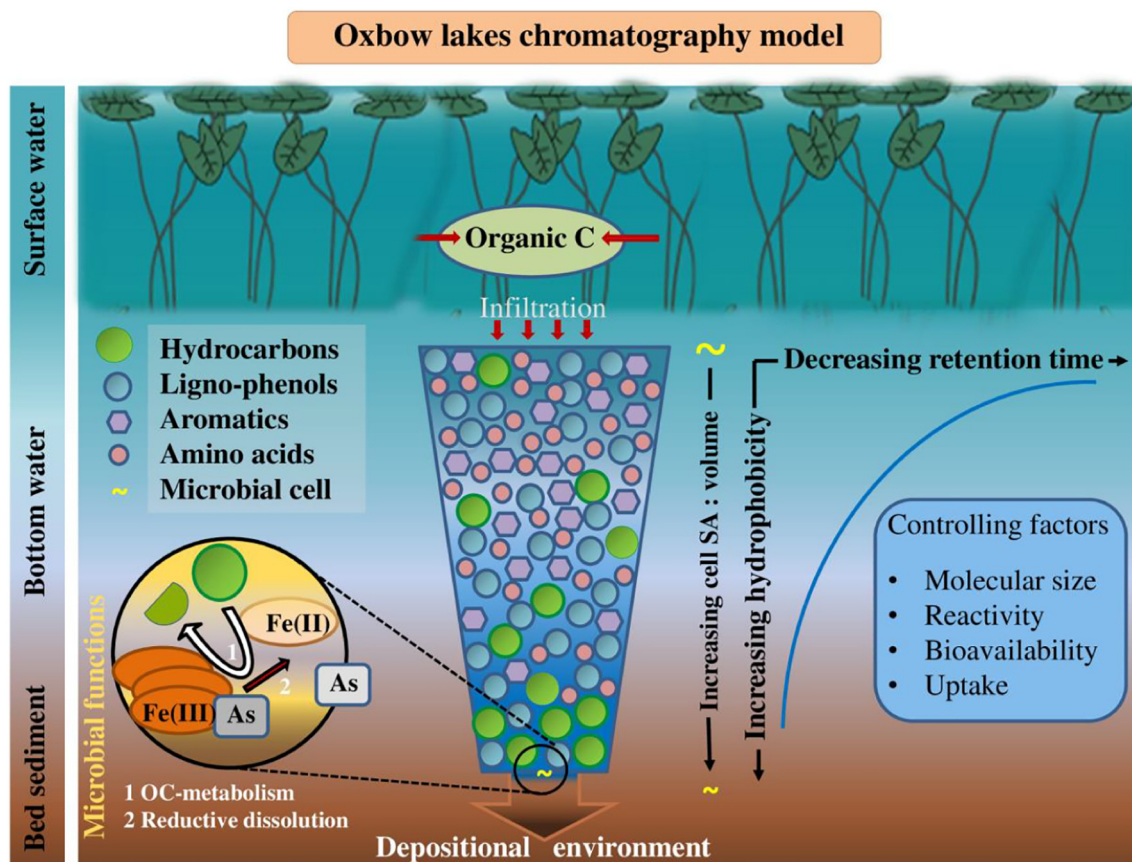

Fig. 9. Oxbow lakes Chromatographic Model: Organic carbon molecules from different sources (macrophytes, terrestrial, anthropogenic) infiltrate through the water column to the saturated redox zone in the bottom. The composition, abundance, and bioavailability of these molecules alter during this transportation by physicochemical and biological metabolic processes. The microbial SA:volume ratio plays a key role in molecular uptake and larger hydrophobic molecules (hydrocarbons) are less preferred relative to ligno-phenols which have hydrophilic and hydrophobic moieties. Hydrocarbons are preferentially partitioned into clay minerals and retain longer. Whereas very small aromatic molecules, although are hydrophobic but are relatively more bioavailable/biodegradable. Amino acids are even smaller, mostly hydrophilic molecules, have lowest retention time in the presented model. The deposition of organic molecules over the time and their metabolism plays a role in natural selection of microbial communities and their redox functions. Eventually controlling the elemental (As, Fe) fluxes in the aquifers.

water inducing change in microbial community dynamics and metabolic functions affecting soil mineral chemistry, results in the infiltration of the molecules through the water column and the eventual shelf life and deposition (Ling et al., 2004; Ghosh et al., 2015a).

The clay minerals and metal oxy-hydroxides play a role in retention and/or diagenesis. The chemical structure of hydrophobic compounds (water-insoluble) such as alkane-hydrocarbons, aromatic groups have strong affinity for humic acids binding to clay minerals (kaolinites; Spencer et al., 2010; Glodowska et al., 2020). The surface area: volume ratio of microbial cell plays a key role in uptake of bioavailable OC molecules. Further, the bioavailability of aromatic compounds is greater than the aliphatic hydrocarbons. This results in the gradient in distribution of the molecules, along the water and sedimentary column (Fig. 9). The $\delta^{18}O$ and δ^2H combined with ^3H tracers had detected the infiltration of the OC (<50 yr) from surface water into shallow aquifers (Saha et al., 2011). Sources are mostly large hydrophobic molecules bound with transitional heavy metals (Fe^{3+} or Pb^{2+}, sequestering terrestrial input. With the annual vegetation decay and deposition, and low energy state, a reducing niche develops in the sediment below the hypolimnion water column. The HMW hydrophobic molecules have a lower bioavailability in the depositional environment, which slows down the redox biogeochemical metabolic transformation and is conducive for progressive release of elements- Fe and As into subsurface water (Fig. 9).

6. Conclusions

The critical role of abandoned-river channels forming oxbow lakes in As hotspots is discussed in this paper. The geomorphological juxtaposition of (a) abandoned channels (or: *oxbow lakes*) where the cocktail of organic matter and As-containing sediment leads to the release of As from its solid state, and (b) the topographically-higher point bars where the released As accumulates in the aquifer and is consumed by the inhabitants, provides a blueprint to explain the origin and localization of As toxicity. A multidisciplinary approach has been effective in understanding the geomorphology of river meanders, forming abandoned channels, which can act a growth bed for biomass. While acting as an incubator for primary production (lake vegetation dynamics), and subsequent organic debris accumulation (anoxic, hypolimnion water column), where a selective preferential preservation of organic carbon compound classes (anoxic sediment base) occur. The manuscript describes the organic compounds infiltration, deposition and abundance depends on their hydrophobicity, molecular weights and bioavailability and further, due to diagenetic alteration (microbial metabolic oxidation). Different classes of surface derived organic carbon from vegetation (terrestrial plants and macrophytes) with anthropogenic input (surrounding villages and agricultural practices), can have different effects on the mineral weathering and in controlling the downstream cationic fluxes such as, Fe, Mn, F etc. and contamination of aquifers in various river plains across the world. The study provides a conceptual organic carbon transport model, which can lead researchers working on other As and other heavy metal-affected Holocene alluvial systems (e.g., Vietnam, Indonesia, Bangladesh, China, Argentina, Bolivia and other parts of India) to explore the possible organic controls on arsenic sources and sinks.

Supplementary data to this article can be found online at https://doi.org/10.1016/j.scitotenv.2020.144400.

CRediT authorship contribution statement

Devanita Ghosh: Conceptualization, Methodology, Investigation, Formal analysis, Writing – original draft, Funding acquisition. **Santosh Kumar:** Investigation, Data curation, Writing – review & editing. **Marinus Eric Donselaar:** Conceptualization, Investigation, Data curation, Writing – review & editing, Funding acquisition. **Cynthia Corroto:** Visualization, Writing – review & editing. **Ashok K. Ghosh:** Conceptualization, Funding acquisition.

Declaration of competing interest

The authors declare that they have no known competing financial interests or personal relationships that could have appeared to influence the work reported in this paper.

Acknowledgements

References

Ader, M., Jézéquel, D., Agrinier, P., 2006. Improved method for isotopic and quantitative analysis of dissolved inorganic carbon in natural water samples. Rapid Commun. Mass Sp. 20, 2243–2251. https://doi.org/10.1002/rcm.2585.

Annaduzzaman, M.D., Rietveld, L., van Halem, D., 2018. Faecal contamination of drinking water in arsenic affected area of rural Bihar: tubewell and storage container survey. In: Zhu, Y., Guo, H., Bhattacharya, P., Ahmad, A., Bundschuh J., Naidu, R. (Eds.), Environmental Arsenic in a changing world. CRC Press Press/Balkema, Leiden, the Netherlands, pp. 502-503.

Assayag, N., Rivé, K., Ader, M., Jézéquel, D., Agrinier, P., 2006. Improved method for isotopic and quantitative analysis of dissolved inorganic carbon in natural water samples. Rapid Commun. Mass Sp. 20, 2243–2251. https://doi.org/10.1002/rcm.2585.

Baig, J.A., Kazi, T.G., Shah, A.Q., Kandhro, G.A., Afridi, H.I., Arain, M.B., Jamali, M.K., Jalbani, N., 2000. Speciation and evaluation of arsenic in surface water and groundwater samples: a multivariate case study. Ecotoxicol. Environ. Saf. 73, 914–923. https://doi.org/10.1016/j.ecoenv.2010.01.002.

Berg, M., Stengel, C., Trang, P.T.K., Hung Viet, P., Sampson, M.L., Leng, M., Samreth, S., Fredericks, D., 2007. Magnitude of arsenic pollution in the Mekong and Red River Deltas - Cambodia and Vietnam. Sci. Total Environ. 372, 413–425. https://doi.org/10.1016/j.scitotenv.2006.09.010.

Bhattacharya, P., Chatterjee, D., Jacks, G., 1997. Occurrence of arsenic-contaminated groundwater in alluvial aquifers from delta plains, eastern India: options for safe drinking water supply. Int. J. Water Resour. Dev. 13, 79–92. https://doi.org/10.1080/07900629749944.

Bhattacharya, P., Jacks, G., Ahmed, K.M., Routh, J., Khan, A.A., 2002. Arsenic in groundwater of the Bengal Delta Plain aquifers in Bangladesh. Bull. Environ. Contam. Toxicol. 69, 538–545. https://doi.org/10.1007/s00128-002-0095-5.

Bhattacharya, P., Claesson, M., Bundschuh, J., Sracek, O., Fagerberg, J., Jacks, G., Martin, R.A., Storniolo, A., Thir, J.M., 2006. Distribution and mobility of arsenic in the Río Dulce alluvial aquifers in Santiago del Estero Province. Argentina. Sci. Total Environ. 358, 97–120. https://doi.org/10.1016/j.scitotenv.2005.04.048.

Bhattacharya, A.K., Mandal, S.N., Das, S.K., 2008. Heavy metals accumulation in water. Sediment and Tissues of Different Edible Fishes in Upper Stretch of Gangetic West Bengal. Trends Appl. Sci. Res. 3, 61–68. https://doi.org/10.3923/tasr.2008.61.68.

Bridge, J.S., 2003. Rivers and Floodplains. Blackwell, Oxford, U.K., 491 p.

BSRDC Ltd., 2016. IND: Bihar New Ganga Bridge Project – Environmental Impact Assessment. Bihar State Road Development Corporation Limited, Government of Bihar for the Asian Development Bank. 333 p.

Bundschuh, J., Farias, B., Martin, R., Storniolo, A., Bhattacharya, P., Cortes, J., Bonorino, G., Albouy, R., 2004. Groundwater arsenic in the Chaco-Pampean Plain, Argentina: case study from Robles county, Santiago del Estero Province. Appl. Geochem. 19, 231–243. https://doi.org/10.1016/j.apgeochem.2003.09.009.

Campbell, J.R., Craw, D., Frew, R., Horton, T., Chamberlain, C.P., 2004. Geochemical signature of orogenic hydrothermal activity in an active tectonic intersection zone, Alpine Fault, New Zealand. Mineral. Deposita 39, 437–451. https://doi.org/10.1007/s00126-004-0421-4.

Carter, V., Rybicki, N.B., Landwehr, J.M., Turtora, M., 1994. Role of weather and water quality in population dynamics of submerged macrophytes in the tidal Potomac River. Estuaries. 17, 417–426. https://doi.org/10.2307/1352674.

Chakraborty, M., Manjunath, K.R., Panigrahy, S., Kundu, N., Parihar, J.S., 2005. Rice crop parameter retrieval using multi-temporal, multi-incidence angle Radarsat SAR data. ISPRS J. Photogramm. 59, 310–322. https://doi.org/10.1016/j.isprsjprs.2005.05.001.

Chari, S., Jonna, S., Raju, P., Murthy, C., Hakeem, K.A., 1994. System Performance Evaluation and Diagnostic Analysis of Canal Irrigation Projects. Proc. of the 15th ACRS, Bangalore. https://a-a-r-s.org/proceeding/ACRS1994/Papers/WR94-2.htm.

Chikkanna, A., Ghosh, D., Kishore, A., 2018. Expression and characterization of a potential exopolysaccharide from a newly isolated halophilic thermotolerant bacteria *Halomonas nitroreducens* strain WB1. PeerJ 6, e4684. https://doi.org/10.7717/peerj.4684.

Chikkanna, A., Mehan, L., Sarath, P.K., Ghosh, D., 2019. Arsenic Exposures, Poisoning, and Threat to Human Health: Arsenic Affecting Human Health. In: Papadopoulou, P., Marouli, C., Misseyanni, A. (Eds.), Environmental Exposures and Human Health Challenges, 1st ed. IGI Global, pp. 86-105. doi:https://doi.org/10.4018/978-1-5225-7635-8.ch004.

Costa, M., 2004. Use of SAR satellites for mapping zonation of vegetation communities in the Amazon floodplain. Int. J. Rem. Sens. 25, 1817–1835. https://doi.org/10.1080/0143116031000116985.

Cranwell, P.A., Eglinton, G., Robinson, N., 1987. Lipids of aquatic organisms as potential contributors to lacustrine sediments. Org. Geochem. 11, 513–527. https://doi.org/10.1016/0146-6380(87)90007-6.

Dietrich, M., Best, K.B., Raff, J.L., Ronay, E.R., 2020. A first-order geochemical budget for suspended sediment discharge to the Bay of Bengal from the Ganges-Brahmaputra river system. Sci. Total Environ. 726, 138667. https://doi.org/10.1016/j.scitotenv.2020.138667.

Donselaar, M.E., Overeem, I., 2008. Connectivity of fluvial point bar deposits: an example from the Miocene Huesca Fluvial Fan, Ebro Basin, Spain. AAPG Bull. 92, 1109–1129. https://doi.org/10.1306/04180807079.

Donselaar, M.E., Bhatt, A.G., Ghosh, A.K., 2017. On the relation between fluvio-deltaic flood basin geomorphology and the wide-spread occurrence of arsenic pollution in shallow aquifers. Sci. Total Environ. 574, 901–913. https://doi.org/10.1016/j.scitotenv.2016.09.074.

Evans, T., Costa, M., Telmer, K., Silva, T., 2010. Using ALOS/PALSAR and RADARSAT-2 to map land cover and seasonal inundation in the Brazilian Pantanal. IEEE J. Sel. Top. Appl. 3, 560–575.

FAO, IAH, UNESCO, World Bank, 2015. Final Report of the Global Groundwater Governance Project. Accessed from:, http://www.groundwatergo-vernance.org..

Fletcher, J., Willby, N., Oliver, D.M., Quilliam, R.S., 2020. Phytoremediation using aquatic plants. In: Shmaefsky, B. (Ed.), Phytoremediation. Concepts and Strategies in Plant Sciences. Springer, Cham https://doi.org/10.1007/978-3-030-00099-8_7.

Ghosh, D., Bhadury, P., 2018. Microbial Cycling of Arsenic in the Aquifers of Bengal Delta Plains (BDP). In: Adhya, T.K., Lal, B., Mohapatra, B., Paul, D., Das, S. (Eds.), Advances in Soil Microbiology: Recent Trends and Future Prospects, 1st ed, Springer Singapore, pp 91-108. doi:https://doi.org/10.1007/978-981-10-6178-3_5.

Ghosh, D., Biswas, J.K., 2015. Biomonitoring macrophytes diversity and abundance for rating aquatic health of an oxbow lake ecosystem in Ganga River Basin. Am. J. Phytomed. Clin. Ther. 3, 602–621.

Ghosh, D., Bhadury, P., Routh, J., 2014. Diversity of arsenite oxidizing bacterial communities in arsenic-rich deltaic aquifers in West Bengal. India. Front. Microbiol. 5, 1–14. https://doi.org/10.3389/fmicb.2014.00602.

Ghosh, D., Routh, J., Bhadury, P., 2015a. Characterization and microbial utilization of dissolved lipid organic fraction in arsenic impacted aquifers (India). J. Hydrol. 527, 221–233. https://doi.org/10.1016/j.jhydrol.2015.04.051.

Ghosh, D, Routh, J, Bhadury, P, 2017. Sub-surface biogeochemical characteristics and its effect on arsenic cycling in the Holocene grey sand aquifers of the Lower Bengal Basin. Front Environ. Sci. 5, 82. https://doi.org/10.3389/fenvs.2017.00082.

Ghosh, D., Routh, J., Dario, M., Bhadury, P., 2015b. Elemental and biomarker characteristics in a Pleistocene aquifer vulnerable to arsenic contamination in the Bengal Delta Plain. India. Appl. Geochem. 61, 87–98. https://doi.org/10.1016/j.apgeochem.2015.05.007.

Ghosh, D., Bhadury, P., Routh, J., 2018. Coping with arsenic stress: Adaptations of arsenite oxidizing bacterial membrane lipids to increasing arsenic levels. MicrobiologyOpen., e594 https://doi.org/10.1002/mbo3.594.

Glodowska, M., Stopelli, E., Schneider, M., Lightfoot, A., Rathi, B., Straub, D., Patzner, M., Duyen, V.T., Members, AdvectAs Team, Berg, M., Kleindienst, S., Kappler, A., 2020. Role of in situ natural organic matter in mobilizing As during microbial reduction of FeIII-mineral-bearing aquifer sediments from Hanoi (Vietnam). Environ. Sci. Technol. https://doi.org/10.1021/acs.est.9b07183.

Gnanaprakasam, E.T., Lloyd, J.R., Boothman, C., Ahmed, K.M., Choudhury, I., Bostick, B.C., van Geen, A., Mailloux, B.J., 2017. Microbial Community Structure and Arsenic Biogeochemistry in Two Arsenic-Impacted Aquifers in Bangladesh. mBio. 8, e01326-17; doi:https://doi.org/10.1128/mBio.01326-17.

Göd, R., Zemann, J., 1999. Native arsenic - realgar mineralization in marbles from Saualpe, Carinthia, Austria. Mineral. Petrol. 70, 37–53.

Guha Mazumder, D.N., 2003. Chronic arsenic toxicity: clinical features, epidemiology, and treatment: experience in West Bengal. J. Environ. Sci. Health A Tox. Hazard. Subst. Environ. Eng. 38, 141–163. https://doi.org/10.1081/ESE-120016886.

Horton, T.W., Becker, J.A., Craw, D., Koons, P.O., Chamberlain, C.P., 2001. Hydrothermal arsenic enrichment in an active mountain belt: Southern Alps, New Zealand. Chem. Geol. 177, 323–339.

Huang, G., Sun, J., Ying, Z., Jing, J., Zhang, Y., Liu, J., 2011. Distribution of arsenic in sewage irrigation area of Pearl River Delta. China. J. of Earth Sci. 22, 396–410. https://doi.org/10.1007/s12583-011-0192-7.

Jones, D.T., Taylor, W.R., Thornton, J.M., 1992. The rapid generation of mutation data matrices from protein sequences. Comput. Appl. Biosci. 8, 275–282. https://doi.org/10.1093/bioinformatics/8.3.275.

Jonna, S., Abdul Hakeem, K., Murthy, C.S., Raju, P.V., Chari, S.T., 1995. Evaluation of simulated IRS-1C WiFS data for concurrent monitoring of command areas at disaggregated level. J. Indian Soc. Remote Sens. 23, 185–194. https://doi.org/10.1007/BF03024499.

Kaiser, K., Benner, R., 2008. Major bacterial contribution to the ocean reservoir of detrital organic carbon and nitrogen. Limnol. Oceanogr. 53, 99–112. https://doi.org/10.4319/lo.2008.53.1.0099.

Kaiser, K., Benner, R., 2012. Characterization of lignin by gas chromatography and mass spectrometry using a simplified CuO oxidation method. Anal. Chem. 84, 459–464. https://doi.org/10.1021/ac202004r.

Kaiser, K., Guggenberger, G., Haumaier, L., 2004. Changes in dissolved lignin-derived phenols, neutral sugars, uronic acids, and amino sugars with depth in forested Haplic Arenosols and Rendzic Leptosols. Biogeochemistry 70, 135–151. https://doi.org/10.1023/B:BIOG.0000049340.77963.18.

Kaiser, C., Franklin, O., Dieckmann, U., Richter, A., 2014. Microbial community dynamics alleviated stoichiometric constraints during litter decay. Ecol. Lett. 17, 680–690. https://doi.org/10.1111/ele.12269.

Kavil, S.P., Ghosh, D., Pašić, I., Routh, J., 2020. Temporal dynamics of arsenic uptake and distribution: food and water risks in the Bengal basin. Toxicol. Environ. Chem. https://doi.org/10.1080/02772248.2020.1767781.

Kawasaki, N., Benner, R., 2006. Bacterial release of dissolved organic matter during cell growth and decline: molecular origin and composition. Limnol. Oceanogr. 51, 2170–2180. https://doi.org/10.4319/lo.2006.51.5.2170.

Lane, D.J., 1991. 16S/23S rRNA sequencing. In: Stackebrandt, E., Goodfellow, M. (Eds.), Nucleic Acid Techniques in Bacterial Systematics. John Wiley & Sons, New York, pp. 115–175.

Lawson, M., Polya, D.A., Boyce, A.J., Bryant, C., Mondal, D., Shantz, Ballentine, C.J., 2013. Pond-derived organic carbon driving changes in arsenic hazard found in Asian groundwaters. Environ. Sci. Technol. 47, 7085–7094. https://doi.org/10.1021/es400114q.

Ling, W., Xu, J., Gao, Y., Wang, H., 2004. Influence of dissolved organic matter (DOM) on environmental behaviors of organic pollutants in soils. Ying Yong Sheng Tai Xue Bao. 15, 326–330.

Louchouarn, P., Opsahl, S., Benner, R., 2000. Isolation and quantification of dissolved lignin from natural waters using solid-phase extraction and GC/MS. Anal. Chem. 72, 2780–2787. https://doi.org/10.1021/ac9912552.

Mukherjee, A., Fryar, A.E., Thomas, W.A., 2009. Geologic, geomorphic and hydrologic framework and evolution of the Bengal basin. India and Bangladesh. J. Asian Earth Sci. 34, 227–244. https://doi.org/10.1016/j.jseaes.2008.05.011.

Mukherjee, A., Verma, S., Gupta, S., Henke, K.R., Bhattacharya, P., 2014. Influence of tectonics, sedimentation and aqueous flow cycles on the origin of global groundwater arsenic: paradigms from three continents. J. Hydrol. 518, 284–299. https://doi.org/10.1016/j.jhydrol.2013.10.044.

Navalgund, R.R., Jayaraman, V., Roy, P.S., 2007. Remote sensing applications: an overview. Curr. Sci. 93, 1747–1766. www.jstor.org/stable/24102069.

Nowak, M.E., Schwab, V.F., Lazar, C.S., Behrendt, T., Kohlhepp, B., Totsche, K.U., Küsel, K., Trumbore, S.E., 2017. Carbon isotopes of dissolved inorganic carbon reflect utilization of different carbon sources by microbial communities in two limestone aquifer assemblages. Hydrol. Earth Syst. Sci. 21, 4283–4300. https://doi.org/10.5194/hess-21-4283-2017.

Nübel, U., Pichel, F.G., Muyzer, G., 1997. PCR primers to amplify 16S rRNA genes from cyanobacteria. Appl. Environ. Microbiol. 63, 3327–3332.

Oblinger, J.L., Koburger, J.A., 1975. Understanding and teaching the most probable number technique. J. Milk Food Technol. 38, 540–545. https://doi.org/10.4315/0022-2747-38.9.540.

Preiner, S., Dai, Y., Pucher, M., Reitsema, R.E., Schoelynck, J., Meire, P., Hein, T., 2020. Effects of macrophytes on ecosystem metabolism and net nutrient uptake in a groundwater fed lowland river. Sci.Tot. Environ. 721, 137620. https://doi.org/10.1016/j.scitotenv.2020.137620.

Ramos, O.E., Rötting, T.S., French, M., Sracek, O., Bundschuh, J., Quintanilla, J., Bhattacharya, P., 2014. Geochemical processes controlling mobilization of arsenic and trace elements in shallow aquifers and surface waters in the Antequera and Poopó mining regions, Bolivian Altiplano. J. Hydrol. 518, 421–433. https://doi.org/10.1016/j.jhydrol.2014.08.019.

Ray, S.S., Dadhwal, V.K., Navalgund, R.R., 2002. Performance evaluation of an irrigation command area using remote sensing: a case study of Mahi command, Gujarat. India. Agric. Water Manag. 56, 81–91. https://doi.org/10.1016/S0378-3774(02)00006-9.

Kumar, S., Ghosh, D., Donselaar, M.E., Burgers, F., Ghosh, A.K., (submitted) Clay-plug sediment as the locus of arsenic in Holocene alluvial plains: quantification of the pollution problem.

Ray, S.S., Mamatha Neetu, S., Gupta, S., 2015. Use of Remote Sensing in Crop Forecasting and Assessment of Impact of Natural Disasters: Operational Approaches in India. In: Srivastava, M.K. (Ed.), Proceedings of FAO Expert meeting on crop monitoring for improved food security. Vientiane, Lao PDR. Food and Agriculture Organization of the United Nations and the Asian Development Bank, Bangkok, pp. 111-121.

Ribbes, F., Le Toan, T., 1999. Rice field mapping and monitoring with RADARSAT data. Int. J. Remote Sens. 20, 745–765. https://doi.org/10.1080/014311699213172.

Rontani, J.F., Volkman, J.K., 2003. Phytol degradation products as biogeochemical tracers in aquatic environments. Org. Geochem. 34, 1–35. https://doi.org/10.1016/S0146-6380(02)00185-7.

Rowland, H.A.L., Polya, D.A., Lloyd, J.R., Pancost, R.D., 2006. Characterization of organic matter in a shallow reducing arsenic rich aquifer, West Bengal. Org. Geochem. 37, 1101–1114. https://doi.org/10.1016/j.orggeochem.2006.04.011.

Saha, D., Sinha, U.K., Dwivedi, S.N., 2011. Characterization of recharge processes in shallow and deeper aquifers using isotopic signatures and geochemical behavior of groundwater in an arsenic enriched part of the Ganga Plain. Appl. Geochem. 26, 432–443. https://doi.org/10.1016/j.apgeochem.2011.01.003.

Sahai, B., Kalubarme, M.H., Javad, K.L., 1985. Ecological studies in the Ukai command area. Int. J. Remote Sens. 6, 401–409. https://doi.org/10.1080/01431168508948462.

Sahu, S., Saha, D., 2015. Role of shallow alluvial stratigraphy and Holocene geomorphology on groundwater arsenic contamination in the Middle Ganga Plain. India. Environ. Earth Sci. 73, 3523–3536. https://doi.org/10.1007/s12665-014-3637-3.

SIS, 1993 Swedish Standard Method SS 02 81 50. Vattenundersökningar – Bestämning av metaller med atom-absorptions spektrometri i flamma – Allmänna principer och regler (Translatedtitle – Water analyses – Metal analyses by flame atomic absorption spectroscopy – Principles and methods).

Spencer, R.G.M., Hernes, P.J., Ruf, R., Baker, A., Dyda, R.Y., Stubbins, A., Six, J., 2010. Temporal controls on dissolved organic matter and lignin biogeochemistry in a pristine tropical river, Democratic Republic of Congo. J. Geophys. Res. Biogeosci. 115, G03013. https://doi.org/10.1029/2009jg001180.

Srivastava, S., Srivastava, A.K., Singh, B., Suprasanna, P., D'Souza, S.F., 2013. The effect of arsenic on pigment composition and photosynthesis in *Hydrilla verticillata*. Biol. Plant. 57, 385–389.

Stecher, G., Tamura, K., Kumar, S., 2020. Molecular Evolutionary Genetics Analysis (MEGA) for macOS. Mol. Biol. Evol. 37, 1237–1239. https://doi.org/10.1093/molbev/msz312.

Sutherland, R.A., 1998. Loss-on-ignition estimates of organic matter and relationships to organic carbon in fluvial bed sediments. Hydrobiologia 389, 153–167. https://doi.org/10.1023/A:1003570219018.

Tapia, J., Murray, J., Ormachea, M., Tirado, N., Nordstrom, D.K., 2019. Origin, distribution, and geochemistry of arsenic in the Altiplano-Puna plateau of Argentina, Bolivia, Chile, and Perú. Sci. Total Environ. 678, 309–325. https://doi.org/10.1016/j.scitotenv.2019.04.084.

Valverde, A., Delvasto, P., Peix, A., Velazquez, E., Santa-Regina, I., Ballester, A., Rodriguez-Barrueco, C., Garcia-Balboa, C., Igual, J.M., 2006. *Burkholderia ferrariae* sp. nov., isolated from an iron ore in Brazil. Int. J. Syst. Evol. Microbiol. 56, 2421–2425. https://doi.org/10.1099/ijs.0.64498-0.

Weishaar, J.L., Aiken, G.R., Bergamaschi, B.A., Fram, M.S., Fujii, R., Mopper, K., 2003. Evaluation of specific ultraviolet absorbance as an indicator of the chemical composition and reactivity of dissolved organic carbon. Environ. Sci. Technol. 37, 4702–4708. https://doi.org/10.1021/es030360x.

World Health Organization (WHO), 2011. Guidelines for Drinking-Water Quality. 4th ed. Geneva, 541 p.

Wu, W., Ruan, J., Ding, S., Zhao, L., Xu, Y., Yang, H., Ding, W., Pei, Y., 2014. Source and distribution of glycerol dialkyl glycerol tetraethers along lower Yellow River estuary–coast transect. Mar. Chem. 158, 17–26. https://doi.org/10.1016/j.marchem.2013.11.006.

Yan, C., Wang, Z., Luo, Z., 2014. Arsenic efflux from *Microcystis aeruginosa* under different phosphate regimes. PLoS One 9, e116099. https://doi.org/10.1371/journal.pone.0116099.

Zhang, Z., Zhao, M., Yang, X., Wang, S., Jiang, X., Oldfield, F., Eglinton, G., 2004. A hydrocarbon biomarker record for the last 40 kyr of plant input to Lake Heqing, southwestern China. Org. Geochem. 35, 595–613. https://doi.org/10.1016/j.orggeochem.2003.12.003.